Layer-stripes in charge-ordered $La_{1-x}Ca_xMnO_3$ (x = 1/3,1/2, and 2/3)

2007 J. Phys.: Condens. Matter 19 106216

(http://iopscience.iop.org/0953-8984/19/10/106216)

IOP PUBLISHING JOURNAL OF PHYSICS: CONDENSED MATTER

J. Phys.: Condens. Matter **19** (2007) 106216 (13pp) doi:10.1088/0953-8984/19/10/106216

Layer-stripes in charge-ordered $La_{1-x}Ca_xMnO_3$ ($x = 1/3$, $1/2$, and $2/3$)

F L Tang and X Zhang

Laboratory of Advanced Materials, Department of Materials Science and Engineering, Tsinghua University, Beijing 100084, People's Republic of China
and
National Center for Electron Microscopy (Beijing), Tsinghua University, Beijing 100084, People's Republic of China

E-mail: xzzhang@tsinghua.edu.cn

Received 19 October 2006, in final form 30 January 2007
Published 23 February 2007
Online at stacks.iop.org/JPhysCM/19/106216

Abstract

Using atomistic simulation we investigated another possible and energetically stable charge-ordering model in $La_{1-x}Ca_xMnO_3$ ($x = 1/3$, $1/2$, and $2/3$): the layer-stripe model, which can coexist with other charge-ordering models and may be a general phenomenon in these compounds. As x increases from $1/3$ to $1/2$ then to $2/3$, the stability of charge ordering increases, which agrees well with experimental results. The stability of the layer-stripe will reduce when its thickness increases; this may be due to the increase of Jahn–Teller distortions. It is also found that the internal structures (lattice spacing and Jahn–Teller distortion) of layer-stripes are inhomogeneous.

1. Introduction

In many transition-metal oxides, charge ordering (CO) seems a general phenomenon and it is important because some electronic/magnetic properties of these compounds are dominated by the coexistence of several ordered phases [1–4]. The real-space charge-ordering models in doped manganites have recently attracted much interest.

Early in the 1950s, Wollan and Koehler [5] proposed the conception of Mn^{3+}/Mn^{4+} charge ordering in $La_{1/2}Ca_{1/2}MnO_3$ and suggested four charge-ordering models with the simple perovskite structure (figures 1(a)–(d)). (For simplicity, we denote these four models as $WK^{(a)-(d)}$ hereafter.) After the finding of colossal magnetoresistance in doped manganites, many authors proposed some other charge-ordering crystal models. Hotta *et al* studied two types of charge ordering: the Wigner crystal (figure 1(e)) and bi-stripe (figure 1(f)) models at $x = 2/3$ with topological concepts [6]. The diagonal stripes [1, 7, 8] at $x \leqslant 1/2$ or at $x = 2/3$ were theoretically presented. Chen and co-workers [9, 10] reported electron microscopy images of $La_{1-x}Ca_xMnO_3$ ($x = 1/2, 2/3$, and $3/4$), and illustrated these images by a paired stripe crystal model. With *ab initio* calculations, the paired stripe model with

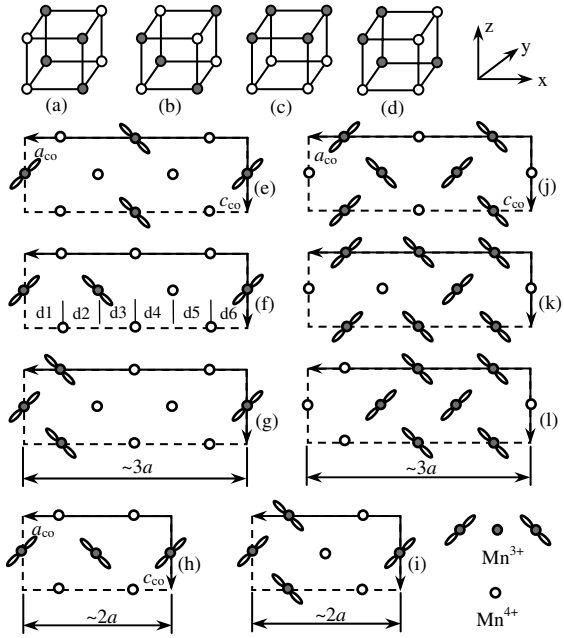

Figure 1. Charge-ordering models of $WK^{(a)-(d)}$ (a)–(d). Wigner crystal (e), bi-stripe (f), and layer-stripe (g) at $x = 2/3$. Charge-ordering models of paired stripe (identical to diagonal stripe and $WK^{(a)}$) (h) and layer-stripe (i) at $x = 1/2$. Wigner crystal (j), bi-stripe (k), and layer-stripe (l) at $x = 1/3$. In (f), $d1$–$d6$ are distances along a_{CO} direction between two adjacent Mn ions.

$x = 1/2$, and Wigner crystal and bi-stripe models with $x = 2/3$, were used to reveal the origin of charge ordering [11, 12]. Ahn and Millis [13] proposed three charge-ordering patterns for $R_{1/2}A_{1/2}MnO_3$ (R: rare-earth elements; A: Ca, Sr or Ba), which are identical to $WK^{(a)-(c)}$, respectively. In fact, when $x = 1/2$, the diagonal stripe model [7, 8] is $WK^{(a)}$, and the paired stripe model (figure 1(h)) can be obtained by rotating $WK^{(a)}$ by 45° around the z-axis.

We have investigated the atomic distribution in $La_{1/3}Ca_{2/3}MnO_3$ and proposed another possible charge-ordering model, the layer-stripe (figure 1(g)) model [14], apart from the Wigner crystal and bi-stripe charge-ordering models. Then a question arises: can the layer-stripe model exist in Ca-doped manganites with other different doping densities? The structure of the layer-stripe needs further investigation. In addition, the effect of doping density on charge ordering seems important but lacking. In this study, we performed atomistic simulations on layer-stripe, Wigner crystal, bi-stripe, and $WK^{(a)-(d)}$ charge-ordering models in $La_{1-x}Ca_xMnO_3$ ($x = 1/3, 1/2$). We compared their structural stability in terms of lattice energies, and studied their most possible structures by comparing their calculated structures with experimental results. The internal structure of layer-stripes is also discussed.

2. Simulation method

The crystal structure of a material at a given temperature and pressure can be predicted by minimizing its free energy. Our approach is to adjust the cell volume and atomic positions until the net pressure or stress is zero. The pressure P is simply the derivative of the free energy F with respect to volume V. Thus for a cubic material:

$$P = \mathrm{d}F/\mathrm{d}V. \tag{1}$$

Calculating the free energy at a given volume and then recalculating it after making a small adjustment to the cell volume dV determines the pressure.

During the iterative procedure, a constant volume energy minimization is performed. Hence, each time the cell volume is modified, all atomic positions are adjusted so that they remain at a potential energy minimum. Thus by minimizing to constant pressure and including the vibrational component of the free energy, the crystal structure at a given temperature and pressure can be predicted. This technique has been used for simulation of many kinds of material [14–16]. Details of this technique are available in [17].

Our simulation is based on the widely used successful shell-model [18] generalization of the Born model of a solid. With this model, the lattice energy E can be expressed as

$$E = \frac{1}{2}\sum_{i,j}\left[\frac{q_i q_j}{r_{ij}} + V(r_{ij})\right], \tag{2}$$

where the first term is the Coulombic energy introduced by long-range interactions of effective charges, and the second term is the short-range interactions. Short-range interaction is represented by a Buckingham potential:

$$V(r) = A\exp(-r/\rho) - Cr^{-6}, \tag{3}$$

where A, ρ, and C are fitting parameters. In order to describe the polarization of an individual ion and its dependence on the local atomic environment, it is treated by the core–shell model [18]. The interaction between the core and shell of any ion is treated as being harmonic with a spring constant k, and is represented by

$$E_v(d_i) = \tfrac{1}{2}kd_i^2, \tag{4}$$

where d_i is the relative displacement of the core and shell of ion i. The polarization of a massless shell with charge Y and a core with charge X ($X + Y$ is the charge of the ion) can be calculated as

$$\alpha = \frac{Y^2}{k}, \tag{5}$$

where Y relates to the dielectric constant, and k is the force constant between the core and the shell, relating to the phonon frequency. Both parameters Y and k are fitting parameters.

The potential parameters for $LaMnO_3$ (table 1) and $CaMnO_3$ (table 2) are obtained at 0 K by an empirical method, known as the 'relaxed' fitting approach: the structure is relaxed to zero strain for every evaluation of the sum of squares and the difference between the observed and calculated structural parameters is used in place of the derivatives. In each step in the fitting, the minimization is started from the experimental structure to avoid the possibility that the fit becomes trapped in an undesirable local minimum in either potential of geometry space.

As atomistic simulation strongly depends on the validity of the potential model used, we have checked the reliability of the potential used in this work. The potential parameters of $LaMnO_3$ and $CaMnO_3$ can reproduce the experimental crystal structure of $LaMnO_3$ or $CaMnO_3$ with differences in the lattice parameters between the calculated and experimental data of less than 1.0% [14]. We have calculated the pressure effect on $LaMnO_3$ up to 3.4 GPa for further testing these potential parameters. When $P < 3.5$ GPa, the calculated compressibilities of V, a, b, and c are 10.0×10^{-3}, 9.0×10^{-3}, -0.12×10^{-3}, and 1.1×10^{-3} GPa^{-1}, respectively. The corresponding experimental values are 8.1×10^{-3}, 6.1×10^{-3}, 0.96×10^{-3}, and 1.3×10^{-3} GPa^{-1}, respectively [19]. The calculated results of the compressibility are in agreement with the experimental results except for the compressibility of the lattice parameter b, indicating that the potentials we used can represent the crystal structure of $LaMnO_3$. We have also investigated the temperature effect on $La_{1-x}Ca_xMnO_3$ ($x = 1/3$, $1/2$, and $2/3$) and

Table 1. Potential parameters for $LaMnO_3$: short-range interaction and shell-model parameters.

	Short-range interaction		
	A (eV)	ρ (Å)	C (eV Å^6)
$O(1)^{2-}$–$O(1)^{2-}$	22 764.3000	0.1490	43.0
$O(2)^{2-}$–$O(2)^{2-}$	22 764.3000	0.1490	43.0
$O(1)^{2-}$–$O(2)^{2-}$	22 764.3000	0.1490	43.0
La^{3+}–$O(1)^{2-}$	2 800.0828	0.3274	0.0
La^{3+}–$O(2)^{2-}$	23 533.3281	0.2447	0.0
Mn^{3+}–$O(1)^{2-}$	8 474.5750	0.2392	0.0
Mn^{3+}–$O(2)^{2-}$	344.0376	0.4431	0.0
	Shell-model parameters		
Species	$Y(e)$	K (eV Å^{-2})	
La^{3+}	−0.250	145.0	
Mn^{3+}	3.000	95.0	
$O(1)^{2-}$	−2.389	42.0	
$O(2)^{2-}$	−2.389	42.0	

Table 2. Potential parameters for $CaMnO_3$: short-range interaction and shell-model parameters.

	Short-range interaction		
	A (eV)	ρ (Å)	C (eV Å^6)
$O(1)^{2-}$–$O(1)^{2-}$	22 764.3000	0.1490	43.0
$O(2)^{2-}$–$O(2)^{2-}$	22 764.3000	0.1490	43.0
$O(1)^{2-}$–$O(2)^{2-}$	22 764.3000	0.1490	43.0
Ca^{2+}–$O(1)^{2-}$	32 525.0215	0.2148	0.0
Ca^{2+}–$O(2)^{2-}$	26 312.4043	0.2197	0.0
Mn^{4+}–$O(1)^{2-}$	16 526.0604	0.2218	0.0
Mn^{4+}–$O(2)^{2-}$	16 741.0424	0.2217	0.0
	Shell-model parameters		
Species	$Y(e)$	K (eV Å^{-2})	
Ca^{2+}	2.0000	110.2	
Mn^{4+}	4.000	95.0	
$O(1)^{2-}$	−2.389	42.0	
$O(2)^{2-}$	−2.389	42.0	

found that the potentials are stable and suitable at low temperature (<100 K). The above lattice, pressure, and temperature effect checks indicate that our potentials can represent the interaction between ions in Ca-doped $LaMnO_3$.

3. Results and discussion

3.1. Layer-stripes and other CO models

First, for completeness, we provide the main results of simulation on $La_{1-x}Ca_xMnO_3$ at $x = 2/3$ in figure 2; the details have been published elsewhere [14]. The layer-stripe model (figure 1(g)) has the lowest lattice energy, and has the closest cell volume to experimental volume [20–24] compared with the Wigner crystal (figure 1(e)) and bi-stripe (figure 1(f))

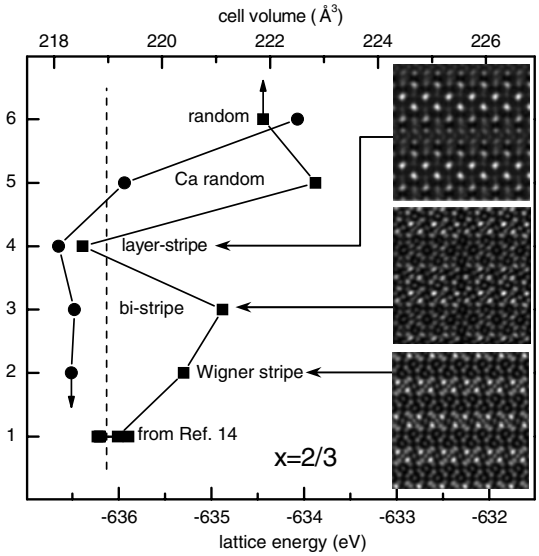

Figure 2. Simulated lattice energy (circle), cell volume (rectangle), and calculated HREM images at $x = 2/3$ for different configurations. The broken line marks the average value of the experiment cell volumes.

models. Ca random configurations, in which Ca ions are randomly distributed but Mn ions are ordered as a Wigner crystal, bi-stripe, or layer-stripe, have higher lattice energy (denoted as E_{Ca}). The random configurations, in which both Ca and Mn ions are randomly distributed, have the highest lattice energy (denoted as E_{R}). The difference between the lattice energies of Wigner crystal, bi-stripe, and layer-stripe is less than 0.2 eV. The calculated high-resolution electronic microcopy (HREM) images for the Wigner crystal, bi-stripe, and layer-stripe models show good charge-ordering stripe contrasts.

Second, we illustrate the atomistic simulation results of $La_{1-x}Ca_xMnO_3$ at $x = 1/2$ in figure 3. Before doing this, it is necessary to introduce the charge-ordering models we simulated. If one extends figure 1(h) (identical to WK$^{(a)}$) along the c_{CO}-axis direction periodically, Mn^{3+} and Mn^{4+} ions will form charge-ordered stripes: these are called 3434 stripes in this paper (3 denotes a Mn^{3+} stripe and 4 denotes a Mn^{4+} stripe along the c_{CO} direction; and it is noticed that the first and the second Mn^{3+} stripes have perpendicular 'orbital' directions). Figure 1(i) denotes another possible Mn ion configuration: the layer-stripe model 3344. If one adopts a larger charge-ordering unit cell, a thick layer-stripe model 333444 (or 33334444) can be obtained. In Ca random configurations, Ca ions are randomly distributed but Mn ions are orderly distributed as 3434, 3344, or 333444. In the random configurations, both Ca and Mn ions are randomly distributed. In the charge-ordering configurations, the Ca ions are arranged near the Mn^{4+} ions for electric neutrality, resulting in Ca ordering along with Mn^{3+}/Mn^{4+} charge ordering.

Figure 3 gives the experimental cell volumes [25–27] with an average volume of $\sim$225 Å^3. WK$^{(a)}$ has a lattice energy of -616.58 eV, and a cell volume of 226.81 Å^3, which is larger than the average experimental volume. WK$^{(b)}$ has higher lattice energy and larger cell volume. WK$^{(c)}$ has much lower lattice energy and much larger cell volume. WK$^{(d)}$ has the lowest lattice energy and a closer volume to the experimental volume. Layer-stripe 3344 has lower lattice energy and the closest volume to the experimental volume. The thicker layer-stripe

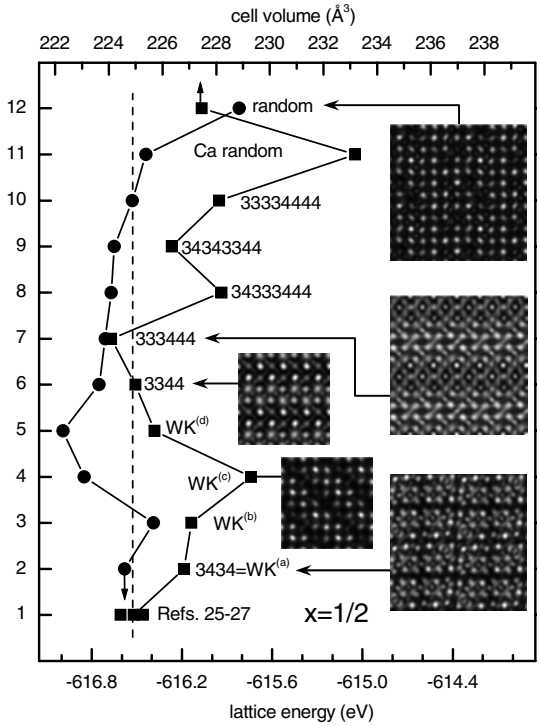

Figure 3. Simulated lattice energy (circle), cell volume (rectangle), and calculated HREM images at $x = 1/2$ for different configurations. The broken line marks the average value of the experiment cell volumes.

333444 has lower lattice energy and small volume. The thickest layer-stripe in this work, 33334444, has higher lattice energy and larger cell volume. Interestingly, one can find that the lattice energy of 333444 is larger than that in 3344, and smaller than that in 33334444, indicating that the stability of the layer-stripe will reduce with increasing thickness. For layer-stripes 3344 and 333444, our calculated Mn–O1 (along the b axis) and Mn–O2 (in the a–c planes) bond lengths are 1.924 Å and 1.972 Å, while the experimental Mn–O1 and Mn–O2 bond lengths were 1.915 Å and 1.957 Å (at 1.54 K) [28], respectively. The difference between them is less than 1%, indicating that our simulation results can represent the internal structures of $La_{1/2}Ca_{1/2}MnO_3$. We also found two 'mixed' charge-ordering models: 34343344 (from WK$^{(a)}$ and 3344) and 34333444 (from WK$^{(a)}$ and 333444). These mixed models have intermediate lattice energies between those of their parent models but larger cell volumes. The Ca random configurations have higher lattice energy (E_{Ca}) and the largest volume, far away from the experimental volume. The random configurations have the highest lattice energy (E_R) and large volume, departing from the experimental volume significantly. The lattice parameters of different configurations are compared with some experimental results in table 3. The layer-stripes 3344 and 333444 have closer lattice parameters to experimental values than other charge-ordering models.

Some typical HREM images for $x = 1/2$ were calculated, and they are shown in figure 3. The 3434 image (WK$^{(a)}$) shows weak charge-ordering character. Image WK$^{(c)}$ shows obvious stripes along the [101] direction. Images WK$^{(b),(d)}$ (not shown) do not show stripe character. Layer-stripe 3344 manifest a good charge-ordering stripe character with a period

Table 3. Simulated and experimental lattice parameters of $La_{1/2}Ca_{1/2}MnO_3$.

	a (Å)	b (Å)	c (Å)
Random[a]	5.4983	7.5531	5.4789
Ca random[b]	5.6274	7.4381	5.5724
WK$^{(a)}$	5.5336	7.5645	5.4184
WK$^{(b)}$	5.5302	7.5574	5.4333
WK$^{(c)}$	5.5708	7.5096	5.4812
WK$^{(d)}$	5.4747	7.5624	5.4517
3344[c]	5.4680	7.5450	5.4536
333444[d]	5.4598	7.5641	5.4270
34333444[e]	5.4977	7.5476	5.4549
34343344[f]	5.5104	7.5337	5.4970
33334444[g]	5.5369	7.4764	5.5109
Experiment[h]	5.4763	7.5247	5.4466
Experiment[i]	5.4309	7.6400	5.4211
Experiment[j]	5.4352	7.6446	5.4241

[a] Average results of random configurations, in which La/Ca and Mn ions are all disordered.
[b] Average results of La/Ca disordered configurations, in which Mn^{3+}/Mn^{4+} are ordered in WK$^{(a)}$, 3344, and 333444.
[c] Average results of layer-stripes 3344 along the a and c directions.
[d] Average results of layer-stripes 333444 along the a and c directions.
[e] Average results of mixed charge-ordering models 34333444 along the a and c directions.
[f] Average results of mixed charge-ordering models 34343344 along the a and c directions.
[g] Layer-stripe 33334444 along the c direction.
[h] Reference [25].
[i] Reference [26].
[j] Reference [27].

of $\sim 2a \approx 11.5$ Å. So do the layer-stripe 333444 stripes with a period $\sim 3a \approx 16.5$ Å. The calculated image of layer-stripe 3344 is similar to the description of experimental charge ordering [10] at $x = 1/2$: layer-stripe 3344 and the experimental stripe have the same period of $\sim 2a$, and have inverted contrast density in one period. The image for the random configuration does not manifest charge-ordering character, but the local structure in one place is different from that in another. As shown in figure 3, layer-stripe 3344 or 333444 has a lower lattice energy, its volume is very close to the experimental results, and its HREM image shows a good charge-ordering stripe contrast. All these indicate that the layer-stripe model may be another structurally possible and energetically stable charge-ordering crystal model for $x = 1/2$, besides WK$^{(a)-(d)}$.

If one denotes the direction with the largest Mn^{3+}–O bond length as the 'orbital' of Mn^{3+} ions (the bond length is closely associated with the d_{z^2} orbital direction [9] of Mn^{3+} ions) in 33 stripes (figure 1(i)), one can find that the first Mn^{3+} stripe has 'orbitals' orientated perpendicularly to the second one, in agreement with the 'orbitals' direction in the charge-ordering models [7, 9, 10] given by Mori *et al*. In addition, considering the orbital direction, our 3434 model (the Mn^{3+} ions 'orbital' direction is denoted by the largest Mn^{3+}–O bond) is identical to the model shown in figure 1(h).

Finally, we illustrate the atomistic simulation results of $La_{1-x}Ca_xMnO_3$ at $x = 1/3$ in figure 4. At this doping density, it was theoretically proved that charge ordering (diagonal stripe) is possible [1, 7]. We can obtain three types of charge-ordering stripe at $x = 1/3$, and for convenience still call them the Wigner crystal (433433) (figure 1(j)), bi-stripe (434333) (figure 1(k)), and layer-stripe (443333) (figure 1(l)), respectively. In these three models the positions of Mn^{3+} and Mn^{4+} ions are obtained by exchanging Mn^{3+} and Mn^{4+} ions in the

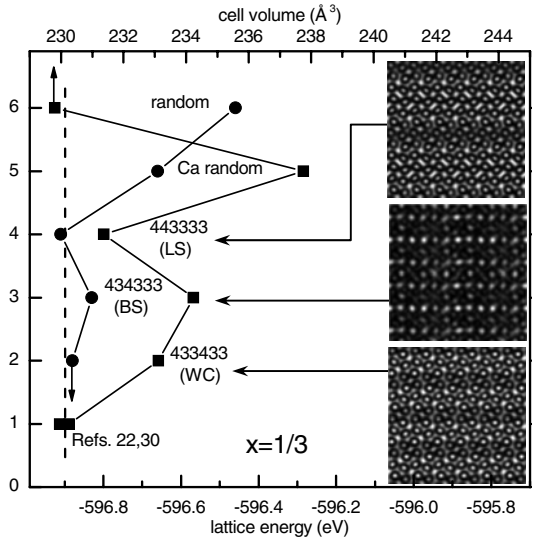

Figure 4. Simulated lattice energy (circle), cell volume (rectangle), and calculated HREM images at $x = 1/3$ for different configurations. The broken line marks the average value of the experiment cell volumes.

Wigner crystal, bi-stripe, and layer-stripe at $x = 2/3$ (figures 1(e)–(g)). We notice that our Wigner crystal model can be obtained by rotating the diagonal stripe with $x = 1/3$ by 45° [1, 7]. Our layer-stripe is similar to the experimental structure of $La_{2/3}Ca_{1/3}MnO_3$ reported in [29]: the La-site ordered films consisted of two pseudocubic unit-cell layers of $LaMnO_3$ and one pseudocubic unit-cell layer of $CaMnO_3$. In figure 4, the layer-stripe has the lowest lattice energy and the closest volume to the experimental volume [26, 30], compared with the Wigner crystal and bi-stripe. It seems that the conception of a layer-stripe is also suitable for $x = 1/3$. The Ca random configurations have higher lattice energy (E_{Ca}), and their volumes depart from the average experimental data dramatically. The random configurations have the highest lattice energies (E_R), and their volumes also depart from the average experimental data significantly. These results are similar to those at $x = 2/3$, but the contrasts in HREM images at $x = 1/3$ (figure 4) are weaker than that at $x = 2/3$. The lattice parameters of different configurations are compared with some experimental results in table 4. The layer-stripe has closer lattice parameters to experimental values compared with the Wigner crystal and bi-stripe.

Our simulation results of $La_{1-x}Ca_xMnO_3$ at $x = 1/3, 1/2$ and $2/3$ show that the layer-stripe models have lower lattice energies with energy difference less than 0.2 eV compared with other charge-ordering stripe models, the closest cell volumes to the experimental results, and a good charge-ordering stripe contrast in HREM images. Therefore, the layer-stripe model may be a general charge-ordering model in $La_{1-x}Ca_xMnO_3$. The small energy difference (<0.2 eV) between different charge-ordering models means that the layer-stripe can coexist with other charge-ordering phases. Radaelli *et al* explained the multi-phases in $La_{1/2}Ca_{1/2}MnO_3$ by more than four coexisting discrete phases with different lattice parameters [28]. Mori *et al* found paired stripes with periodicities of $3a$ and $5a$ as defect structures of the normal $4a$ stripes in the samples with $x = 3/4$ [10]. In samples with $x = 5/8$, the charge-ordering state was a fine mixture of $2a$ stripes and $3a$ stripes, and their frequency was governed completely by the level rule. Our simulations found that $La_{1/2}Ca_{1/2}MnO_3$ can contain different periodicity stripes: $2a$ stripes of 3434 or 3344, and $3a$ stripe of 333444. These experimental and simulated results

Table 4. Simulated and experimental lattice parameters of $La_{2/3}Ca_{1/3}MnO_3$.

	a (Å)	b (Å)	c (Å)
Random[a]	5.5360	7.6018	5.5154
Ca random[b]	5.6672	7.4989	5.5945
Bi-stripe[c]	5.5587	7.5807	5.5588
Wigner-stripe[d]	5.5756	7.5923	5.5047
Layer-stripe[e]	5.5361	7.5923	5.5047
Experiment[f]	5.4720	7.7110	5.4570
Experiment[g]	5.4693	7.7070	5.4556

[a] Average results of random configurations, in which La/Ca and Mn ions are all disordered.
[b] Average results of La/Ca disordered configurations, in which Mn^{3+}/Mn^{4+} are ordered in bi-stripe, Wigner crystal, and layer-stripe.
[c] Average results of bi-stripes along the a and c directions.
[d] Average results of Wigner crystal stripes along the a and c directions.
[e] Average results of layer-stripes along the a and c directions.
[f] Reference [22].
[g] Reference [30].

indicate that the structure of manganite materials is indeed inhomogeneous with coexistence of some different charge-ordering phases.

Our simulations on Ca-doped $LaMnO_3$ demonstrate that the doped cations and Mn^{3+}/Mn^{4+} ions tend to form charge ordering states (even stripes) rather than to be randomly distributed. In charge-ordering states, ions are arranged periodically along some special lattice directions or in some special lattice planes. Charge ordering seems a general phenomenon and has multiple phases at a certain doping density. When one experimentally investigates the atomistic distribution of these compounds, for example, using transmission electronic microcopy, the different charge-ordering states must be taken into account. In addition, a charge- or spin-ordering phenomenon can also be found in other strongly correlated electronic systems, for instance, Na-doped CoO_2 or copper oxide superconductors [2–4]. It was suggested that charge/spin ordering is crucial for understanding high-temperature superconductivity [4]. To study the atomistic distribution and lattice structures in the above compounds, use of the simulation method may be of importance.

3.2. Internal structure of layer-stripes

The internal structure of layer-stripes can be illustrated with the Mn-ion coordinates. In figure 5(a), the layer-stripe of 333444 (with a period $\sim 3a$) is shown schematically; the lattice spacings ($d1$–$d6$) in it are also given. If the stripe 333 or 444 is regarded as a lattice, the lattice parameter of the 333 stripe along the a_{CO}-direction is 5.757 Å, which is slightly larger than the lattice parameter of $LaMnO_3$ (5.739 Å). The lattice parameter of the 444 stripe is 5.152 Å, which is smaller than that of $CaMnO_3$ (5.279 Å). Lattice expansion takes place in the 333 stripe, and lattice contraction in the 444 stripe. Mori *et al* [10] have found lattice contraction in paired stripes and dilation in non-paired stripes in $La_{1/2}Ca_{1/2}MnO_3$ from HREM images. In the layer-stripes, there is a transition layer between 333 and 444 layers ($d3$ or $d6$ in figure 5(a)), and its lattice spacing is smaller than the lattice spacing in the 333 stripe ($d1$ and $d2$) and larger than the lattice spacing in the 444 stripe ($d4$ and $d5$).

These local lattice inhomogeneities can also be seen in the layer-stripe 33334444 (with a period $\sim 4a$) shown in figure 5(b). The lattice parameter of the Mn^{3+} 3333 layer is 5.803 Å, and that of the Mn^{4+} 4444 layer is 5.138 Å. More interestingly, it is found that local lattice inhomogeneities can take place in the Mn^{3+} or Mn^{4+} layer-stripe itself. In figure 5(b), there are three lattice spacings: $d2 < d1 \approx d3$ in the 3333 stripe, and $d6 < d5 \approx d7$ in the

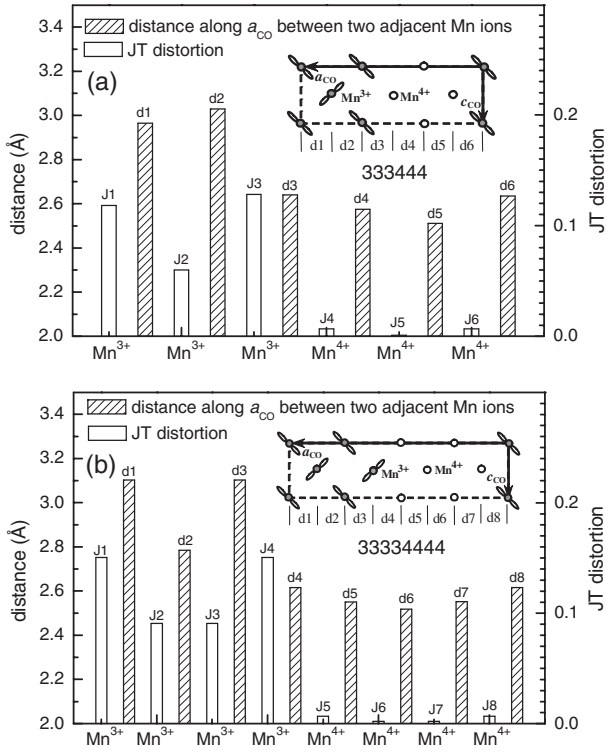

Figure 5. Internal structure (lattice spacing and Jahn–Teller distortion) of layer-stripe 333444 (a) and 33334444 at $x = 1/2$ (b) along the c direction. The Mn^{3+} and Mn^{4+} ions in the bottom of (a) or (b) correspond to the Mn^{3+} and Mn^{4+} ions in the inset, from left to right, respectively. $d1$–$d8$ are distances along the a_{CO} direction between two adjacent Mn ions. $J1$–$J8$ are the Jahn–Teller distortions of Mn^{3+} ions or octahedral distortions around Mn^{4+} ions in the inset.

4444 stripe. These local inhomogeneities can be found along the direction perpendicular to the layer-stripes, and cannot be found along the directions parallel to the layer-stripes. These local inhomogeneities can also be found in other charge-ordering stripes, but not as obviously as that in layer-stripe models. For example, the lattice distances (not shown) in bi-stripe 343444 satisfy $d4 \approx d5 < d1 \approx d2 \approx d3 \approx d6$ (figure 1(f)).

From the experimental lattice parameters of $La_{1/2}Ca_{1/2}MnO_3$ and $La_{1/3}Ca_{2/3}MnO_3$, one can find that the lattice distortion almost disappears: the lattice parameters a, $b/\sqrt{2}$, and c have almost the same value (figure 2(b)). We also found that at $x = 1/2$ the Jahn–Teller distortions in Mn^{3+} stripes still persist, though they are somewhat smaller than that in $LaMnO_3$, but the MnO_6 octahedral distortions in Mn^{4+} stripes are very small (almost zero, figure 5). The calculation method for Jahn–Teller distortion from lattice and MnO_6 octahedral distortions can be seen in [31] and [32]. In the 3333 layer (figure 5(b)), the Jahn–Teller distortions are different for different Mn^{3+} ions: the Jahn–Teller distortion localized on the two inner Mn^{3+} ions ($J2$ and $J3$) is smaller than that on the two outer Mn^{3+} ions ($J1$ and $J4$). If a Mn^{4+} ion is adjacent to a Mn^{3+} ion, its octahedral distortion ($J5$ or $J8$) will be larger, caused by the distortion of the neighbouring Mn^{3+} ions. This finding accords well with other theoretical [33] and experimental [34] results: the Jahn–Teller distortion persists when the crystallographic structure show no lattice distortion. It confirms also that the Jahn–Teller distortions along Mn^{3+} stripes are in fact Jahn–Teller 'sheets' [10].

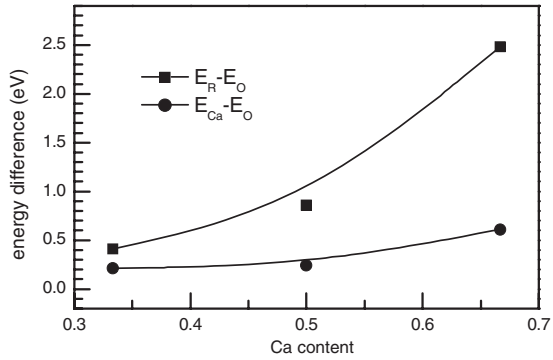

Figure 6. The difference of the lattice energy between random (E_R), Ca random (E_{Ca}), and charge-ordering (E_O) configurations.

We also noted that the Jahn–Teller distortions in the 333444 layer-stripe (figure 5(a)) are smaller than that in the 33334444 stripe (figure 5(b)), but larger than that in the 3344 stripe (not shown). This may be the reason why the lattice energy of the 333444 layer-stripe is smaller than that in the 33334444 stripe, but larger than that in the 3344 stripe (figure 3).

Our simulations on Ca-doped $LaMnO_3$ show that the internal structure of layer-stripes or other charge-ordered phases is inhomogeneous. Ca doping introduces not only charge ordering but also structure ordering: different local structures (including Jahn–Teller 'sheets') emerge periodically in the lattice and the local structure is very different from the average structure (figure 5). In fact, the experimental HREM images of charger-ordered manganites were dominated by the lattice distortions rather than the charge transfer which dominates only at small scatter angles [9, 10]. Local structures are important for electronic/magnetic properties of doped manganites. We have previously calculated the Jahn–Teller energy by lattice distortion and MnO_6 octahedral distortion and estimated bandwidth by bond length and bond angles [32]. The Jahn–Teller energy and bandwidth have a direct effect on the change of the Curie temperature. Additionally, periodical local structures in charge-ordered states will affect the lattice vibration, and then affect the electrons' transport property. This may help in understanding the colossal magnetoresistance in doped manganites.

3.3. CO dependence of doping density

We qualitatively illustrate the stability of charge ordering in $La_{1-x}Ca_xMnO_3$ with different doping densities. From figures 3, 4 and the results for $La_{1/3}Ca_{2/3}MnO_3$, we notice that the difference in lattice energy between random configuration and ordering configuration, $E_R - E_O$, increases from 0.4 to 0.9 to 2.5 eV when $x = 1/3 \rightarrow 1/2 \rightarrow 2/3$ (figure 6), respectively. (E_O is the average lattice energy of 3434, 3344, and 333444 stripes when $x = 1/2$. When $x = 1/3$ or $2/3$, E_O is the average lattice energy of the Wigner crystal, bi-stripe, and layer-stripe.) This phenomenon implies that the stability of charge ordering in $La_{1-x}Ca_xMnO_3$ increases when $x = 1/3 \rightarrow 1/2 \rightarrow 2/3$. This suspicion coincides with the charge-ordering temperature T_{CO} ($x \geqslant 0.5$), which is ~170 K for $La_{1/2}Ca_{1/2}MnO_3$, and ~270 K for $La_{1/3}Ca_{2/3}MnO_3$, respectively [1], indicating that the charge ordering in the former is more easily destroyed than that in the latter upon warming. In addition, it is reported that an external magnetic field can introduce much larger variation in T_{CO} at $x = 0.5$ than that at $x > 0.55$, and the stability of charge ordering in $La_{1-x}Ca_xMnO_3$ increases when x increases from 0.5 to 0.75 [35]. We believe that $La_{2/3}Ca_{1/3}MnO_3$ has a charge-ordering tendency, but with a weak charge-ordering

stability. This may be the reason why charge ordering is seldom found experimentally in $La_{2/3}Ca_{1/3}MnO_3$. Our result is in agreement with the experimental finding: directly imaging of charge ordering in $La_{2/3}Ca_{1/3}MnO_3$ is more difficult than that in $La_{1/3}Ca_{2/3}MnO_3$ [36].

In most experiments, although Ca ions are on average randomly distributed at higher temperatures, little is known about their local arrangement in charge-ordering stripes at low temperatures. We investigate this issue by checking the lattice energy of different Ca distributions. From figures 3, 4 and results in $La_{1/3}Ca_{2/3}MnO_3$, we notice that the difference in lattice energy between the Ca random configuration and ordering configuration, $E_{Ca} - E_O$, is slightly larger than zero when $x = 1/3, 1/2$, and $2/3$ (figure 6). This implies that Ca ions have a small thermodynamic tendency to ordering. Recently, some La-site-ordering manganites have been made [29]. It has been found that if the concentration of Ca is higher in the region above a particular octahedron, the energy of $La_{1/2}Ca_{1/2}MnO_3$ is lowered by 3.8 eV per unit cell [37]. However, the large scale of Ca ion redistribution seems difficult at temperatures around T_{CO}. We suspect that the Ca ordering tendency may be destroyed very easily by a nonequilibrium cooling or warming procedure. We suggest that the Ca distribution deserves to be considered in theoretical treatments of charge ordering in colossal magnetoresistance manganites, at least from the viewpoint that Ca distribution can affect the local structures [37].

4. Conclusion

We investigated another possible and stable charge-ordering model: the layer-stripe model in $La_{1-x}Ca_xMnO_3$ ($x = 1/3, 1/2$, and $2/3$) using atomistic simulation. Compared with other charge-ordering models, it gives lower lattice energy, the closest cell volume to the experimental results, and a good charge-ordering stripe contrast. It can coexist with other charge-ordering stripes, and may be a general phenomenon in these compounds. The internal structures (lattice spacing and Jahn–Teller distortions) of layer-stripes are inhomogeneous. The stability of the layer-stripe will reduce when its thickness increases, and this may be due to the increase of Jahn–Teller distortions. The local Jahn–Teller distortions persist in the Mn^{3+} layer-stripe even when the lattice distortion almost disappears. We found that the charge-ordering stability increases when the doping density $x = 1/3 \rightarrow 1/2 \rightarrow 2/3$. We also found that doped Ca ions have a small tendency to be ordered at lower temperatures (<100 K).

Acknowledgments

The authors would like to thank the Ministry of Science and Technology of China (Grant Nos TG2000067108 and 2002CB613500) and National Science Foundation of China (Grant No. 90401013) for financial support. One of the authors (FLT) would also like to thank Chen Jun for her help in HREM image calculation and Tian Peng for his useful discussion.

References

[1] Dagotto E, Hotta T and Moreo A 2001 *Phys. Rep.* **344** 1
[2] Lee K-W and Pickett W E 2006 *Phys. Rev. Lett.* **96** 96403
[3] Andersen B M and Hedegård P 2005 *Phys. Rev. Lett.* **95** 37002
[4] Dagotto E 2005 *Science* **309** 257
[5] Wollan E O and Koehler W C 1955 *Phys. Rev.* **100** 545
[6] Hotta T, Takada Y, Koizumi H and Dagotto E 2000 *Phys. Rev. Lett.* **84** 2477
[7] Hotta T, Feiguin A and Dagotto E 2001 *Phys. Rev. Lett.* **86** 4922
[8] Brey L 2004 *Phys. Rev. Lett.* **92** 127202
[9] Chen C H, Cheong S-W and Hwang H Y 1997 *J. Appl. Phys.* **81** 4326

[10] Mori S, Chen C H and Cheong S-W 1998 *Nature* **392** 473
[11] Popović Z and Satpathy S 2002 *Phys. Rev. Lett.* **88** 197201
[12] Mutou T and Kontani H 1999 *Phys. Rev. Lett.* **83** 3685
[13] Ahn K H and Millis A J 1998 *Phys. Rev.* B **58** 3697
[14] Tang F L and Zhang X 2006 *Phys. Rev.* B **73** 144401
[15] Catlow C R A, Thomas J M, Parker S C and Jefferson D A 1982 *Nature* **295** 658
[16] Catlow C R A and Price G D 1990 *Nature* **347** 243
[17] Gale J and Rohl A L 2003 *Mol. Simul.* **29** 291
[18] Dick B G and Overhauser A W 1958 *Phys. Rev.* **112** 90
[19] Loa I, Adler P, Grzechnik A, Syassen K, Schwarz U, Hanfland M, Rozenberg G K, Gorodetsky P and Pasternak M P 2001 *Phys. Rev. Lett.* **87** 125501
[20] Fernández-Díaz M T, Martínez J L, Alonso J M and Herrero E 1999 *Phys. Rev.* B **59** 1277
[21] Radaelli P G, Cox D E, Capogna L, Cheong S W and Marezio M 1999 *Phys. Rev.* B **59** 14440
[22] Wang R, Gui J, Zhu Y and Moodenbaugh A R 2000 *Phys. Rev.* B **61** 11946
[23] Pissas M and Kallias G 2003 *Phys. Rev.* B **68** 134414
[24] Wang Y X, Du Y, Qin R W, Han B, Du J and Lin J H 2001 *J. Solid State Chem.* **156** 237
[25] Radaelli P G, Cox D E, Marezio M and Cheong S-W 1997 *Phys. Rev.* B **55** 3015
[26] Rodriguez E E, Proffen T, Llobet A, Rhyne J J and Mitchell J F 2005 *Phys. Rev.* B **71** 104430
[27] Pissas M and Kallias G 2003 *Phys. Rev.* B **68** 134414
[28] Radaelli P G, Cox D E, Marezio M, Cheong S-W, Schiffer P E and Ramirez A P 1995 *Phys. Rev. Lett.* **75** 4488
[29] Palanisami A, Warusawithana M, Eckstein J N, Weissman M B and Mathur N D 2005 *Phys. Rev.* B **72** 24454
[30] Huang Q, Santoro A, Lynn J W, Erwin R W, Borchers J A, Peng J L, Ghosh K and Greene R L 1998 *Phys. Rev.* B **58** 2684
[31] Ahn K H and Millis A J 2001 *Phys. Rev.* B **64** 115103
[32] Tang F L and Zhang X 2005 *J. Phys.: Condens. Matter* **17** 6507
[33] Louca D, Egami T, Brosha E L, Röder H and Bishop A R 1997 *Phys. Rev.* B **56** R8475
[34] Louca D and Egami T 1999 *Phys. Rev.* B **59** 6193
[35] Li X G, Zheng R K, Li G, Zhou H D, Huang R X, Xie J Q and Wang Z D 2002 *Europhys. Lett.* **60** 670
[36] Tao J and Zuo J M 2004 *Phys. Rev.* B **69** 180404(R)
[37] Ferrari V, Towler M and Littlewood P B 2003 *Phys. Rev. Lett.* **91** 227202